Synthesis of Pt-Cu/SiO$_2$ catalysts with different structures and their application in hydrodechlorination of 1,2-dichloroethane

Xing Wei [a,b], Ai-Qin Wang [a], Xiao-Feng Yang [a], Lin Li [a], Tao Zhang [a,*]

[a] State Key Laboratory of Catalysis, Dalian Institute of Chemical Physics, Chinese Academy of Sciences, 116023, PR China
[b] Graduate University of Chinese Academy of Sciences, Beijing, 100049, PR China

ARTICLE INFO

ABSTRACT

Pt-Cu/SiO$_2$ catalysts with different structures and chemical compositions were prepared using a two-step method. For the series of Pt$_x$Cu$_{100-x}$/SiO$_2$ catalysts, Pt was deposited in the first step with H$_2$PtCl$_6$ as the precursor and Cu was deposited subsequently with Cu(NH$_3$)$_4$$^{2+}$ as the precursor. For the Cu$_{100-x}$Pt$_x$/SiO$_2$ catalyst, the deposition sequence was reversed accompanied with galvanic displacement of Cu^0 by Pt^{4+}. All the samples were characterized by XRD, TEM, H$_2$-TPR, H$_2$ chemisorption, and DRIFT of CO adsorption, and evaluated for the catalytic hydrodechlorination of 1,2-dichloroethane. The results show that the Pt$_x$Cu$_{100-x}$/SiO$_2$ catalysts exhibit core–shell structures with Pt-rich alloy cores and Cu-rich alloy shells, while the Cu$_{100-x}$Pt$_x$/SiO$_2$ catalyst shows a Pt–Cu alloy core and a Pt rich alloy shell. Different structures and chemical compositions lead to quite different performances in catalyzing the hydrodechlorination of 1,2-dichloroethane. The Pt$_{16}$Cu$_{84}$/SiO$_2$ catalyst gave a high selectivity to ethylene over 90% and an excellent stability over 18 h run due to the Cu-rich shell structure, while the Cu$_{44}$Pt$_{56}$/SiO$_2$ catalyst produced predominantly ethane due to the Pt rich shell.

© 2012 Elsevier B.V. All rights reserved.

1. Introduction

Chlorinated aliphatic hydrocarbons (CAH) have been widely used in the manufacturing and cleaning industries, and have become one of the most common and harmful contaminants of soil and groundwater due to their persistence in the environment and toxicity [1,2]. Removal of CAH by means of hydrodechlorination has gained much attention because it can convert industrial by-products to valuable chemical feedstocks [3–15]. Hydrogen-assisted dechlorination of 1,2-dichloroethane (DCE) into ethylene is a good example [14,16–23]. For this reaction, bimetallic catalysts such as Pt–Cu [19,21,22,24,25], Pt–Sn [18,20], and Pd–Ag [23,26,27] have been proved to be much more selective towards ethylene than the monometallic noble metals. The high selectivity to ethylene achieved on the bimetallic catalysts was proposed to be attributed to the geometric effect, that is, the dilution effect of IB metal on the IIIV metals resulted in a lower adsorption energy of ethylene and allowed for the easy desorption of ethylene from the active sites [19,25,28,29]. It was also proposed that in a bimetallic catalyst such as Pt–Cu, Cu played a predominant role in catalyzing the C—Cl bond scission and in favoring the desorption of ethylene, while Pt was mainly responsible for providing the adatom H to

regenerate the Cu active sites [19,24,30]. Accordingly, in order to achieve a highly selective catalyst, rational design and synthesis of a Pt–Cu bimetallic catalyst with a Cu-enriched surface is highly desirable.

Co-impregnation followed by reduction treatment is a simple and widely used method for the synthesis of Pt–Cu alloy catalysts [19,21,22,31–33]. However, it often leads to a non-uniform particle size distribution and uncontrollable surface compositions. Recently, some new synthesis methods allowing for well-controlled particles sizes and chemical compositions are emerging [34–39]. For example, Zhou et al. used a polyol reduction method to synthesize Pt–Cu core–shell and alloy nanoparticles and found that Cu@Pt core@shell nanoparticles had a high activity similar to Pt but a significantly higher selectivity to N$_2$ in the NO$_x$ reduction [40]. Xie et al. used dendrimer metal nanocomposites as precursors for the synthesis of SiO$_2$-supported Pt–Cu alloy nanoparticles with a narrow size distribution, and achieved a stable performance with ethylene selectivity exceeding 70% at 275 °C over Pt$_1$Cu$_3$ alloy catalyst [24].

Previously, we developed a two-step method for the synthesis of silica supported Au–Ag [41] and Au–Cu [42–44] bimetallic nanoparticles. A significant advantage of this two-step method is that the deposition of a second metal Ag or Cu suppresses greatly the aggregation of gold nanoparticles during the high-temperature treatment, thus allowing for the synthesis of thermally stable bimetallic nanoparticles. Moreover, the two-step method provides a unique way to tune the structure and chemical composition of

* Corresponding author. Tel.: +86 411 84379015; fax: +86 411 84691570.
E-mail address: taozhang@dicp.ac.cn (T. Zhang).

Table 1
Chemical and phase compositions, and particle sizes of different catalysts.

Sample	Nominal loading (wt.%)		Actual loading[a] (wt.%)		Phase composition[b]	d_{XRD}[c] (nm)	d_{TEM}[d] (nm)
	Pt	Cu	Pt	Cu			
Pt/SiO_2	4.0	–	2.2	–	Pt	8.4	7.8
$Pt_{62}Cu_{38}/SiO_2$	3.6	0.4	2.0	0.4	$Pt_{86}Cu_{14}$, $Pt_{35}Cu_{65}$	6.1	6.0
$Pt_{35}Cu_{65}/SiO_2$	3.0	1.0	1.8	1.1	$Pt_{76}Cu_{24}$, $Pt_{28}Cu_{72}$	5.4	5.6
$Pt_{16}Cu_{84}/SiO_2$	2.0	2.0	1.2	2.1	$Pt_{56}Cu_{44}$, Pt_5Cu_{95}	4.2	4.3
Cu/SiO_2	–	4.0	–	2.7	Cu	2.9	3.1
$Cu_{44}Pt_{56}/SiO_2$	3.0	1.0	2.3	0.6	$Cu_{54}Pt_{46}$, $Cu_{15}Pt_{85}$	4.9	4.6
$Pt_{35}Cu_{65}/SiO_2$-im	1.8	1.1	1.8	1.1	$Pt_{42}Cu_{58}$	–	–

[a] Determined by ICP.
[b] Calculated by Vegard's law.
[c] Calculated by applying Scherrer equation to the main reflections of the alloy cores.
[d] Determined by TEM.

the bimetallic catalysts, depending on the deposition sequence and post-synthesis treatment. In the present work, we extend this two-step method to the synthesis of Pt–Cu bimetallic catalysts with different structures and compositions. Then, with different structured catalysts, we investigate the reaction of hydrodechlorination of DCE to ethylene, and attempt to correlate the catalytic performance with the bimetallic structures.

2. Experimental

2.1. Catalyst preparation

Pt_xCu_{100-x}/SiO_2 (x refers to the atomic percentage of Pt) catalysts were prepared with a two-step method that we previously developed for the synthesis of Au-Ag/SiO_2 [41] and Au-Cu/SiO_2 [42–44] catalysts. In this method, the silica support (Qingdao Ocean Chemical Plant, $S_{BET} = 467\,m^2/g$) was first functionalized with 3-aminopropyltriethoxysilane (APTES, 99%, Acros Organics) according to literature [45,46]. 1 g of the resultant SiO_2–APTES was then added into a certain volume of 0.01 M H_2PtCl_6 solution with a desired Pt loading and stirred for 30 min. After filtration and washing with water, the recovered solid was re-dispersed into 20 mL water, to which 0.2 M $NaBH_4$ was added dropwise under vigorous stirring for reduction of $PtCl_6^{2-}$. After stirring for 20 min, the solid was recovered by filtration and thoroughly washed with water to remove Cl^- for the subsequent Cu deposition, which was the same as the above Pt deposition except that $Cu(NH_3)_4^{2+}$ was used as the precursor. The $Cu(NH_3)_4^{2+}$ solution was prepared by adding 1.25 wt.% ammonia water into 0.02 M $Cu(NO_3)_2$ solution with a molar ratio of NH_3 to Cu 10:1. After deposition of Cu, the solid was calcined at 500 °C in air for 6 h and reduced at 550 °C in H_2 for 1 h to obtain the Pt_xCu_{100-x}/SiO_2 catalyst. For all the catalysts with various Pt/Cu ratios, the total metal loading was fixed at 4 wt.%, but the actual metal loadings may deviate from the nominal values (see Table 1).

For comparison, a $Cu_{44}Pt_{56}/SiO_2$ catalyst was prepared by a reverse deposition sequence to that for Pt_xCu_{100-x}/SiO_2 catalysts with some modifications. In detail, a certain amount of Cu^{2+} was first deposited onto SiO_2–APTES using $Cu(NH_3)_4^{2+}$ as the precursor. After filtration and washing with water, the recovered solid was re-dispersed in water and stirred vigorously under Ar atmosphere, to which 0.2 M $NaBH_4$ was added dropwise and the color of the suspension changed from blue to brown, indicating Cu^{2+} was reduced to Cu^0. After 15 min, a certain amount of 2 wt.% HCl was added until no bubbles produced to ensure the exhaustion of $NaBH_4$ in the solution. Then, an aqueous solution of 0.01 M H_2PtCl_6 was added dropwise into the suspension, and the stirring was continued for 1 h to allow for the galvanic displacement of Cu^0 by Pt^{4+}. After filtration and washing with water, the recovered solid was

dried at 80 °C overnight, calcined at 500 °C in air for 6 h and reduced at 550 °C in H_2 for 1 h.

In comparison with the two-step deposition method, a $Pt_{35}Cu_{65}/SiO_2$-im catalyst with the same Pt and Cu contents as those of $Pt_{35}Cu_{65}/SiO_2$ was synthesized by an incipient wetness impregnation method using H_2PtCl_6 and $Cu(NO_3)_2$ as precursors.

2.2. Catalyst characterization

The actual metal loadings and the Pt/Cu atomic ratios of various Pt_xCu_{100-x}/SiO_2 and $Cu_{44}Pt_{56}/SiO_2$ samples were determined by inductively coupled plasma spectrometer (ICP-AES) on an IRIS Intrepid II XSP instrument (Thermo Electron Corporation).

X-ray powder diffraction (XRD) analysis was carried out on a PANalytical X'pert diffractometer using nickel-filtered Cu Kα radiation with a scanning angle (2θ) of 10–90°, operated at 40 kV and 100 mA.

Transmission electron microscopy (TEM) was carried out with a Tecnai G2 Spirit (FEI) microscope operating at 200 kV, while high-resolution transmission electron microscopy (HRTEM) was conducted with a Tecnai G2 F30 S-Twin (FEI) microscope operating at 300 kV. Before TEM and HRTEM observations, a very little amount of powder sample was ultrasonically dispersed in ethanol and a drop of the dispersion was placed on a microgrid carbon polymer supported on a nickel grid and allowed to dry at room temperature. Chemical compositions of individual particles were determined by energy-dispersive X-ray spectroscopy (EDS) on Tecnai G2 F30 S-Twin (FEI) electron microscope.

Chemisorptions of H_2 were measured using a Micromeritics AutoChem II 2920 instrument with a pulse chemisorption mode. Prior to the measurement, a catalyst sample (80 mg, 20–40 mesh) was reduced in a pure H_2 flow at 550 °C for 1 h followed by purging with Ar flow at 560 °C for 1 h. After cooling to 40 °C under Ar, the gas flow was switched to 10% H_2/Ar to start the H_2 chemisorption. H_2 loop gas was used for each pulse, and several pulses were introduced until saturation. The amount of H_2 was measured with a thermal conductivity detector (TCD).

Temperature programmed reduction (H_2-TPR) experiments were performed on the same instrument as for chemisorption. Prior to the measurements, the samples were pretreated in an Ar flow at 200 °C for 1 h. After cooling to room temperature under Ar, the gas was switched to 10% H_2/Ar and the sample bed was heated to 800 °C at a ramp of 10 °C/min. The consumption of H_2 was determined with TCD.

Diffuse reflectance infrared Fourier transform (DRIFT) spectra were acquired with a BRUKER Equinox 55 spectrometer, equipped with a MCT detector and operated at a resolution of 4 cm^{-1}. Before experiment, a catalyst sample (ca.10 mg) in a powder form was loaded into a reaction cell and then heated to 550 °C at 15 °C/min and held at that temperature for 30 min in a dynamic highly pure H_2

(99.999%) atmosphere, followed by purging with He (20 mL/min) at 550 °C for 30 min. After cooling to the room temperature in He, the spectra collection was started when the probe gas of 2 vol.% CO/He was introduced into the reaction cell at a total flow rate of 20 mL/min. After 20 min, a flow of He (20 mL/min) was switched into the cell. The spectra were recorded at different time at room temperature, and the background of the sample was subtracted to obtain the IR spectrum of adsorbed CO on the catalyst.

2.3. Catalyst evaluation

Hydrodechlorination of DCE was carried out under atmospheric pressure in a tubular quartz micro reactor (4.8 mm), inside which 50 mg of a catalyst sample mixed with 150 mg SiC powder was supported on a fritted disk. The DCE was metered into the reaction system by flowing a sweep gas of He through a VLE saturator filled with the liquid DCE. A constant DCE concentration was ensured by maintaining the saturator at a fixed temperature of 0 °C using an ice-water bath. Prior to the activity measurement, each sample was reduced in a flow of H_2 at 550 °C for 1 h, followed by purging in a flow of Ar for 30 min at the same temperature. After cooling to a certain reaction temperature, the feed gas containing 3.3% DCE, 33% H_2, and balance He was introduced at a flow rate of 30 mL/min, yielding a space velocity of 36,000 $cm^3 g_{cat}^{-1} h^{-1}$. The catalytic activities were measured with time on stream at a fixed temperature. The reaction was run at 275 °C and 350 °C for 18 h and sampling was made every 40 min. Both the inlet and outlet gases were analyzed on line with an Agilent Technologies 6890N gas chromatograph equipped with a FID detector using a 30-m Poraplot Q capillary column. The conversion of DCE (C_{DCE}) was calculated by the equation: C_{DCE} (%) = (moles of all products)/(moles of all products + moles of DCE unconverted) × 100. The selectivity of ethylene ($S_{C_2H_4}$) was calculated by the equation: $S_{C_2H_4}$ (%) = (moles of ethylene produced)/(moles of all products) × 100.

3. Results and discussion

3.1. Synthesis and characterization of Pt_xCu_{100-x}/SiO_2 catalysts

Different from the traditional impregnation method [19,21,22,31,32,47] or colloidal nanoparticle deposition method [24,40,48,49], we employed a two-step method based on a grafting–adsorption–reduction procedure to synthesize silica supported PtCu bimetallic nanoparticles. This method has achieved great success in the synthesis of small sized and uniformly dispersed Au–Ag and Au–Cu nanoparticles on the silica support in our previous work [41–44]. Nevertheless, it encountered some limits in tuning the ratio of two metals since the amount of the second metal deposited onto the surface of the first metal was very limited. In the present work, the Pt/Cu ratios must be tuned in a wide range so as to be applied in the hydrodechlorination of DCE. For this purpose, the previous two-step method has been improved greatly in this work through using a $Cu(NH_3)_4^{2+}$ as the copper precursor. Initially, we tried a series of copper precursors including $Cu(NO_3)_2$, $CuSO_4$, $CuCl_2$, and $Cu(CH_3COO)_2$, but much lower amount of copper than the desired value was deposited. For example, when a Pt/Cu atomic ratio of 35/65 is desired, the actual Pt/Cu atomic ratio was only 88/12 when $Cu(CH_3COO)_2$ was used as the precursor. Taking it into account that the support surface was functionalized with APTES, we finally chose $Cu(NH_3)_4^{2+}$ as the copper precursor with an attempt to deposit copper precursor via the ligand exchange between APTES and NH_3. The result showed that the amount of copper deposited onto the support coincided with the desired value in a wide range of Pt/Cu atomic ratios. As shown in Table 1, $Pt_{62}Cu_{38}/SiO_2$, $Pt_{35}Cu_{65}/SiO_2$, and

$Pt_{16}Cu_{84}/SiO_2$ bimetallic catalysts with controllable Pt/Cu ratios were successfully prepared with this improved method. It was noted that for the pure copper and platinum catalysts (Cu/SiO_2 and Pt/SiO_2), the amounts of copper and platinum deposited onto the support were much lower than the desired values. This might be due to the desired metal loading (4 wt.%) exceeds the maximum copper or platinum amount that can be adsorbed on the support. On the other hand, for the bimetallic Pt_xCu_{100-x}/SiO_2 catalysts, the actual Cu loadings were almost identical to the nominal values, indicating Cu was quantitatively deposited on the preformed Pt/SiO_2 catalyst. Accordingly, it can be speculated that the pre-deposited Pt nanoparticles on the support act as nuclei for the further deposition of Cu component on them. Actually, our previous work on the Au–Ag and Au–Cu nanoparticles has shown that the two-step method resulted in a core@shell like structure, i.e., the gold nanoparticles which were deposited in the first step formed cores while Cu or Ag deposited in the second step formed as shells or patches [41–44]. Analogously, the Pt_xCu_{100-x}/SiO_2 catalysts synthesized in this work probably have a core–shell like structure. Subsequently, we employed a combination of characterization techniques to identify the structures of PtCu bimetallic nanoparticles before and after the reduction treatment.

Fig. 1 shows the XRD patterns of Pt_xCu_{100-x}/SiO_2 catalysts with various Pt/Cu ratios as well as monometallic Pt/SiO_2 and Cu/SiO_2 catalysts under different heat treatment conditions. All the calcined Pt-containing samples present XRD patterns which are characteristic of metallic Pt (PDF code: 00-004-0802). Compared to pure Pt/SiO_2 catalyst, the XRD peaks of Pt_xCu_{100-x}/SiO_2 bimetallic catalysts became broader with an increase of the Cu content, indicative
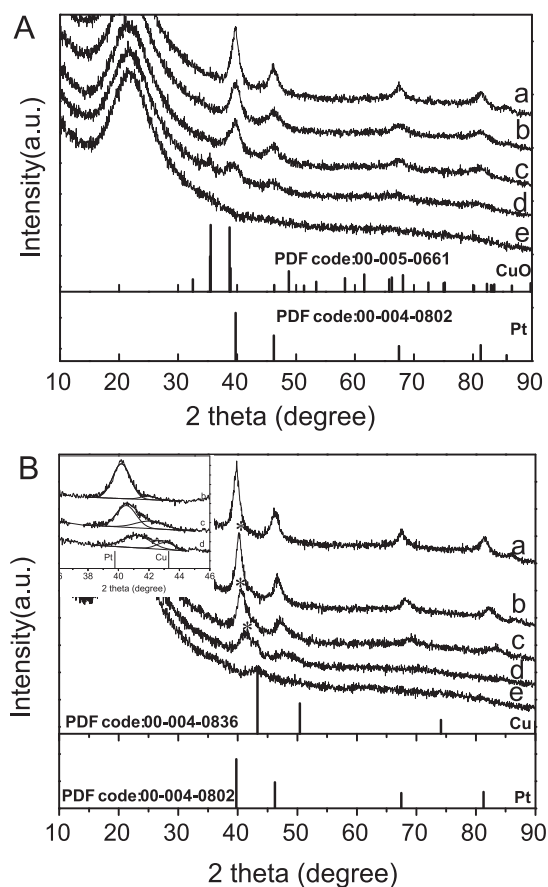

Fig. 1. XRD patterns of Pt_xCu_{100-x}/SiO_2 catalysts after calcination in air at 500 °C (A) and followed with H_2 reduction at 550 °C (B). The inset is the deconvolutions of the XRD peaks denoted with *. x = 100 (a), 62 (b), 35 (c), 16 (d), and 0 (e).
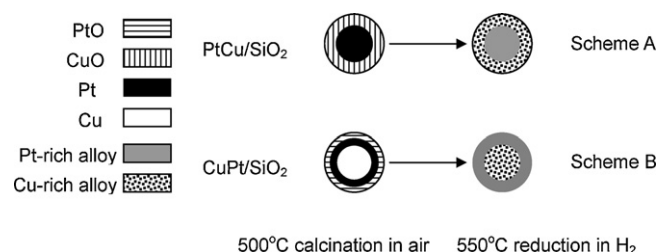
Fig. 2. Schematic illustration of the nanoparticle structures for Pt_xCu_{100-x}/SiO_2 and $CuPt/SiO_2$ catalysts under different treatments.

of the smaller particle sizes. This trend is in accordance with our previous claim that the presence of a second metal suppresses significantly the sintering of particles [41–44]. Moreover, for the three bimetallic Pt_xCu_{100-x}/SiO_2 catalysts, CuO phase could also be identified besides the major phase of metallic Pt, and it appeared more prominent with an increase of the copper content. In contrast, for the pure Cu/SiO_2 catalyst, no any reflection appeared, suggesting the amorphous nature of copper oxides or the too small particle sizes to be detected by XRD. Since the Pt_xCu_{100-x}/SiO_2 catalysts were prepared with a two-step method which has been proved successful in producing Au@CuO core–shell structure [43], it is reasonable to speculate that the calcined Pt_xCu_{100-x}/SiO_2 samples have similar core–shell structures with metallic Pt as the core and CuO as the shell, in accordance with above XRD results. It is this layer of CuO that prevents the sintering of Pt nanoparticles during the calcination process at 500 °C.

After reduction at a high temperature (550 °C), the XRD patterns of the bimetallic catalysts changed greatly. The original Pt peaks shifted towards higher angles with an increase of the Cu contents, meanwhile new peaks appeared at the 2θ positions very close to metallic Cu (see the inset in Fig. 1B) for all the Pt_xCu_{100-x}/SiO_2 bimetallic samples. The former phenomenon can be an indicator of a Pt-rich Pt–Cu alloy phase, while the latter is due to the formation of a Cu-rich Pt–Cu alloy. We used Vegard's law [50] to estimate the chemical compositions of both Pt-rich and Cu-rich alloy phases, and the results are listed in Table 1. It can be seen that the $Pt_{62}Cu_{38}/SiO_2$ catalyst was composed of two alloy phases: $Pt_{86}Cu_{14}$ and $Pt_{35}Cu_{65}$. Similarly, the $Pt_{35}Cu_{65}/SiO_2$ was composed of $Pt_{76}Cu_{24}$ and $Pt_{28}Cu_{72}$, and the $Pt_{16}Cu_{84}/SiO_2$ catalyst was composed of $Pt_{56}Cu_{44}$ and Pt_5Cu_{95} phases. The formation of Pt–Cu alloy phases can be ascribed to the high-temperature reduction process which allows the reduction of CuO_x to metallic Cu followed by interfacial diffusion of Pt and Cu atoms [40,47,51]. Since these three PtCu bimetallic samples are probably in the form of a Pt core covered or decorated with CuO layer/patches before the reduction treatment, the diffusion of Cu atoms towards the Pt core results in the formation of a Pt-rich Pt–Cu alloy core, while the diffusion of Pt atoms towards the surface Cu layer/patches leads to the formation of a Cu-rich layer or patches upon reduction treatment. The structures before and after the reduction treatment are schematically illustrated in Fig. 2.

On the other hand, it is noted that the widths of the XRD peaks remained essentially unchanged before and after the reduction treatment, indicative of the thermally stable particles of the bimetallic catalysts. Applying Scherrer equation to the main reflections of the Pt-rich alloy cores, the average crystal sizes of the Pt-rich cores were estimated to be 6.1 nm, 5.4 nm, and 4.2 nm for $Pt_{62}Cu_{38}/SiO_2$, $Pt_{35}Cu_{65}/SiO_2$, and $Pt_{16}Cu_{84}/SiO_2$, respectively, which were significantly diminished than that of the pure Pt/SiO_2 catalyst (8.4 nm).

Fig. 3 shows the TEM images and particle size distributions of the reduced catalysts. All particles were spherical and uniformly dispersed on the silica support. The average particle sizes,

estimated from more than 200 particles of different areas of each sample, were 7.8 nm, 6.0 nm, 5.6 nm, 4.3 nm, and 3.1 nm for Pt/SiO_2, $Pt_{62}Cu_{38}/SiO_2$, $Pt_{35}Cu_{65}/SiO_2$, $Pt_{16}Cu_{84}/SiO_2$, and Cu/SiO_2, respectively (see Table 1). This trend was in good agreement with the XRD result, demonstrating further the important role of CuO in limiting the aggregation of particles. Examination on many individual particles of the $Pt_{35}Cu_{65}/SiO_2$ sample with EDS shows that each particle contains both Cu and Pt elements (Fig. 4a), confirming the formation of alloy bimetallic structure rather than a mixture of separate Cu and Pt. In addition, from the high-resolution TEM image shown in Figs. 4b and S1 in supplementary material, one can clearly see the core–shell structure of the $Pt_{35}Cu_{65}/SiO_2$ sample. The core has lattice fringes with an interspace of 1.93 Å, which are well consistent with the (1 0 0) plane of the $Pt_{76}Cu_{24}$ alloy phase. The shell appears as an amorphous structure, which is probably caused by the irradiation of high-energy electrons during the HRTEM operations which destruct the crystalline structure of the thin shell. According to the XRD result, this shell should possess a phase composition of $Pt_{28}Cu_{72}$.

The above characterizations provide evidence that the series of Pt_xCu_{100-x}/SiO_2 catalysts have a core–shell like structure with a Pt-rich alloy core and a Cu-rich alloy shell. The presence of Cu has a significant role in limiting the aggregation of nanoparticles during the high-temperature treatment. In the following section, we will demonstrate that this two-step method is also effective for the synthesis of $CuPt/SiO_2$ catalyst with a Cu rich alloy core and a Pt rich alloy shell.

3.2. Synthesis and characterization of $Cu_{44}Pt_{56}/SiO_2$ catalyst

For the synthesis of Cu@Pt core–shell structured nanoparticles, we just use the reverse deposition sequence to that for Pt@Cu core–shell. However, when $PtCl_6^{2-}$ anions were adsorbed on the preformed Cu^0 nanoparticles supported on silica, galvanic displacement of Cu^0 by Pt^{4+} would occur according to the following reaction:

$$2Cu + [PtCl_6]^{2-} \rightarrow Pt + 2Cu^{2+} + 6Cl^-$$
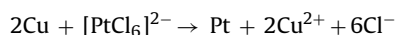
This is because the E^0 of $Pt/[PtCl_6]^{2-}$ is much greater than that of Cu/Cu^{2+} (0.742 V vs. 0.340 V) [52]. To ensure all of the Pt^{4+} species are reduced by Cu^0, an excess amount of copper (0.682 mmol Cu vs. 0.228 mmol Pt^{4+}) was employed in the first step. In this case, the resulting structure would be a Cu@Pt core–shell structure. However, the actual structure is quite different from the expected one. Fig. 5a shows the XRD patterns of the resultant sample. The 500 °C calcined sample presented reflections of PtO and metallic Pt, and no any Cu species were detected by XRD. The mixture phase of PtO and Pt suggests that only the outermost layer of Pt was oxidized while the underlying Pt was protected from the oxidation during the high-temperature calcination. Upon reduction at 550 °C, the PtO peak disappeared while very broad peaks appeared at 2θ values between metallic Pt and metallic Cu which could be deconvoluted into reflections of $Cu_{54}Pt_{46}$ and $Cu_{15}Pt_{85}$ alloys (see Table 1 and the inset in Fig. 5a). This result suggests that during the reduction process, Pt and Cu atoms at the interface respectively diffuse into the copper core and Pt shell, forming Cu-rich alloy core and Pt-rich alloy shell [40,47,51]. The structure of the $Cu_{44}Pt_{56}/SiO_2$ is illustrated in Fig. 2B. Moreover, the $Cu_{44}Pt_{56}/SiO_2$ sample has a uniform particle size distribution with an average particle size of 4.6 nm (Fig. 5b and c).

For comparison, we have also prepared a Pt–Cu alloy catalyst with a co-impregnation method ($Pt_{35}Cu_{65}/SiO_2$-im). After high-temperature reduction treatment, the Pt–Cu alloy formed (see XRD pattern in Fig. 6a) with a phase composition of $Pt_{42}Cu_{58}$ (calculated from Vegard's law), which is very close to the chemical

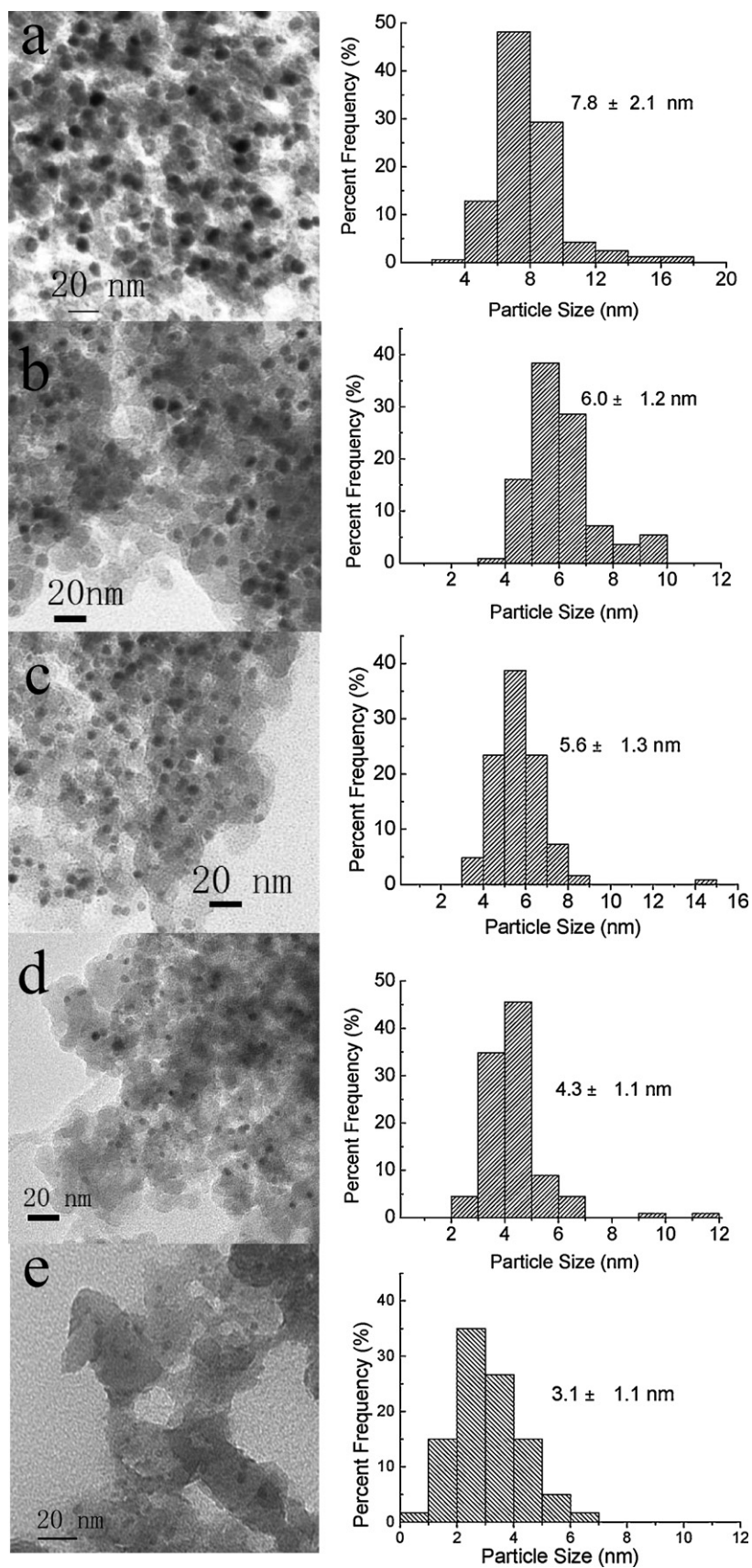**Fig. 3.** TEM images and particle size distributions of Pt_xCu_{100-x}/SiO_2 catalysts: (a) Pt/SiO_2, (b) $Pt_{62}Cu_{38}/SiO_2$, (c) $Pt_{35}Cu_{65}/SiO_2$, (d) $Pt_{16}Cu_{84}/SiO_2$, and (e) Cu/SiO_2.
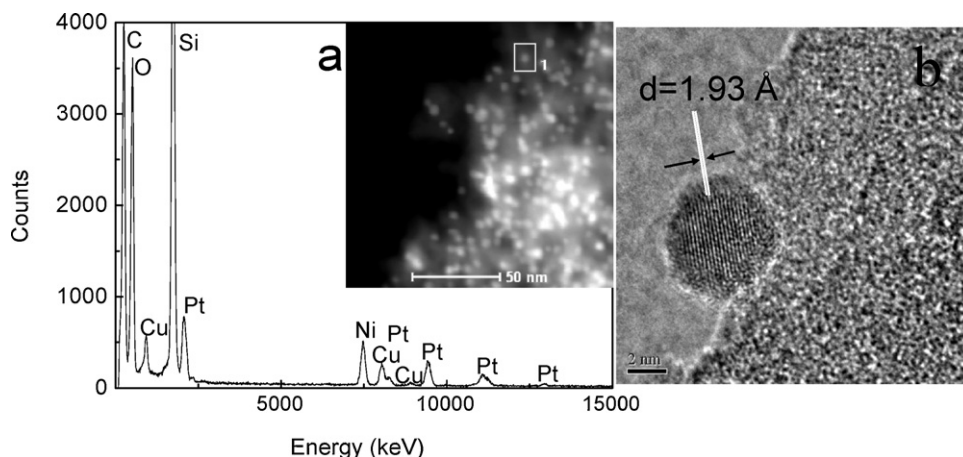
Fig. 4. EDS analysis result (a) and HRTEM image (b) of an individual particle randomly selected on $Pt_{35}Cu_{65}/SiO_2$ catalyst.

composition of the catalyst (see Table 1), indicative of a uniform alloy structure instead of a core–shell structure. On the other hand, this sample presents a rather broad particle size distribution, and severe agglomeration can be clearly seen from TEM images (Fig. 6b). Evidently, in comparison with the co-impregnation, our two-step method presents a remarkable advantage in controlling the particle size of bimetallic nanoparticles.

3.3. H_2-TPR, H_2-chemisorption, and DRIFT of CO adsorption

Fig. 7 shows the H_2-TPR profiles of a series of the calcined Pt_xCu_{100-x}/SiO_2 bimetallic catalysts as well as the $Cu_{44}Pt_{56}/SiO_2$

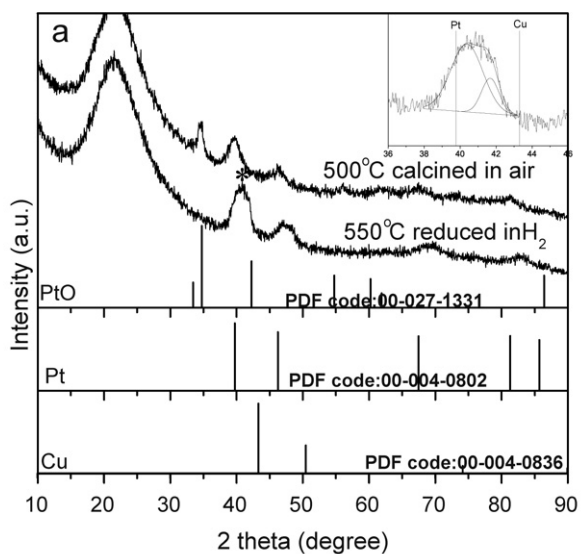**Fig. 5.** XRD patterns (a), TEM image (b), and particle size distribution (c) of the $Cu_{44}Pt_{56}/SiO_2$ catalyst. The inset is the deconvolution of the XRD peak denoted with *.

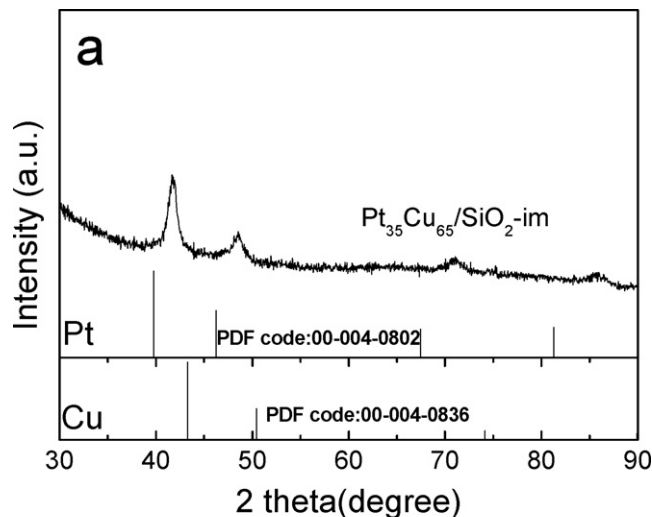**Fig. 6.** XRD pattern (a) and TEM image (b) of $Pt_{35}Cu_{65}/SiO_2$-im catalyst. The inset shows some very small particle on the same sample.

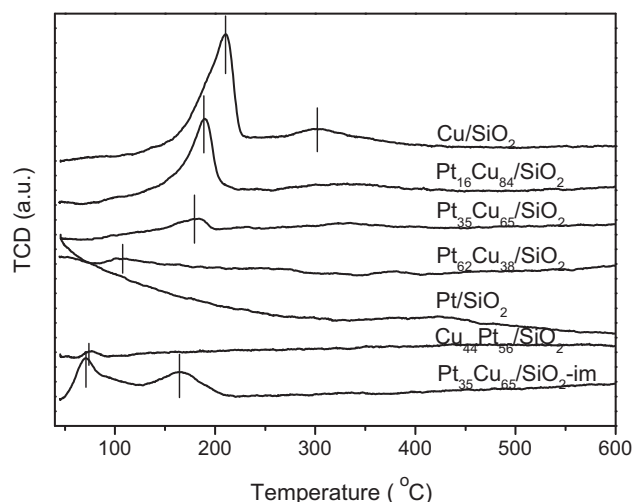**Fig. 7.** H_2-TPR profiles of different Pt–Cu bimetallic catalysts as well as Pt/SiO_2 and Cu/SiO_2 catalysts.

Fig. 8. DRIFT spectra of CO adsorption on different catalysts at room temperature (a); after purging with He for 20 min (b).

and $Pt_{35}Cu_{65}/SiO_2$-im catalysts. For the pure Cu/SiO_2 catalyst, there was a major reduction peak centered at 210 °C and a very minor reduction peak centered at 307 °C. The former can be assigned to the reduction of CuO species which are highly dispersed on the support while the latter to the reduction of bulk CuO [45]. For the $Pt_xCu_{100−x}/SiO_2$ bimetallic catalysts, the first reduction peak shifted to a lower temperature meanwhile its intensity decreased greatly with a decrease of the Cu content. No any peak corresponding to the reduction of PtO_x species was found over $Pt_xCu_{100−x}/SiO_2$ bimetallic samples, in consistence with the Pt@CuO core–shell structure deduced from XRD result. On the other hand, for the pure Pt/SiO_2 catalyst, the reduction occurred even below 40 °C, which can be ascribed to the reduction of PtO_x formed by the oxidation of outmost surface Pt upon exposure to air. Evidently, in the calcined $Pt_xCu_{100−x}/SiO_2$ bimetallic samples, the presence of CuO shell protected the inside Pt^0 from oxidation by exposure to air. The more easily reducible CuO species on the $Pt_xCu_{100−x}$ bimetallic particles than that on pure Cu/SiO_2 can be ascribed to the modification of Pt core on the CuO shell. The thinner is the CuO shell, the more easily reduced it will be. For example, the reduction of CuO_x species of $Pt_{62}Cu_{38}/SiO_2$ sample occurred at a temperature as low as 110 °C. On the other hand, for the $Pt_{35}Cu_{65}/SiO_2$-im catalyst, there were two peaks positioned at 71 °C and 165 °C, which were due to the reduction of PtO and CuO_x, respectively. The different reduction profiles of the $Pt_{35}Cu_{65}/SiO_2$-im catalyst from those of $Pt_xCu_{100−x}/SiO_2$ series of catalyst provides further evidence that the $Pt_xCu_{100−x}/SiO_2$ catalysts are in the Pt@CuO core–shell structure upon high-temperature calcination. For the $Cu_{44}Pt_{56}/SiO_2$ catalyst, only one reduction peak occurs at 75 °C due to the reduction of PtO. The absence of CuO reduction peak implies that the copper is covered by the PtO layer, which is in good agreement with the XRD result that a Cu@Pt core–shell structure forms in the as-synthesized sample. Calculations of the H_2 consumption (Table 2) showed that the amount of H_2 consumed for the reduction of CuO_x species was smaller than that required for the reduction of Cu^{2+} to Cu^0 (i.e.,

Table 2
H_2 consumption for reduction of CuO_x in H_2-TPR experiment.

Sample	H_2 consumption (mmol/g_{cat})	H/Cu[a]
$Pt_{62}Cu_{38}/SiO_2$	0.012 (110 °C)	0.39
$Pt_{35}Cu_{65}/SiO_2$	0.036 (171 °C)	0.42
$Pt_{16}Cu_{84}/SiO_2$	0.130 (190 °C), 0.027 (327 °C)	0.95
Cu/SiO_2	0.211 (210 °C), 0.076 (307 °C)	1.35

[a] Molar ratio of the consumed H to Cu.
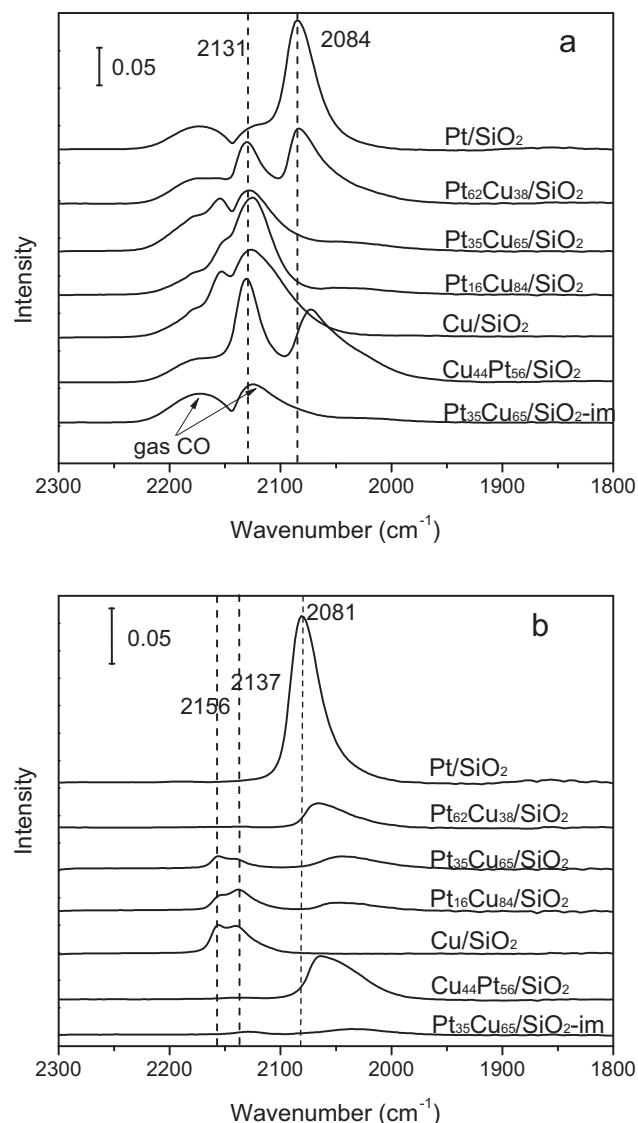
H/Cu molar ratio equals to 2) for most of the Cu-containing catalysts. Moreover, the lower was the Cu content, the smaller was the actual H/Cu ratio. One possible reason is that some Cu^{2+} species have already been reduced to Cu^+ during the pretreatment process considering that the catalysts were pretreated in Ar atmosphere at 200 °C for 1 h prior to the H_2-TPR experiments [53,54], which was also proved by DRIFT spectra of CO adsorption (Fig. S2 in supplementary material). Another possible reason is that some Cu^+ species interacting strongly with the support and acting as the nanoglue between the nanoparticles and silica support cannot be reduced to Cu^0 even after the high-temperature reduction [43] (also see the IR results in Fig. 8b). With an increase of the Cu content, the CuO shell becomes thicker and the percentage of the Cu species interacting strongly with the support will decrease, which leads to the increase of the reducible Cu species. Therefore, we can observe the increasing trend of the H/Cu ratio with an increase of the Cu content.

The H_2-chemisorption data in Table 3 showed that the H_2 uptake on the monometallic Pt/SiO_2 was 11.7 μmol/g_{cat}. For the three $Pt_xCu_{100−x}/SiO_2$ bimetallic catalysts, the H_2 uptakes were greatly decreased following the order of $Pt_{62}Cu_{38}/SiO_2 > Pt_{35}Cu_{65}/SiO_2 > Pt_{16}Cu_{84}/SiO_2$, while it was almost negligible on the monometallic Cu/SiO_2 catalyst because of the

Table 3
H$_2$ chemisorption uptakes and the Pt dispersions of different catalysts.

Sample	H$_2$ chemisorption (μmol/g$_{cat}$)	D_{Pt}[a] (%)	D_{TEM}[b] (%)	$[D_{Pt}]/D_{TEM}$[c]
Pt/SiO$_2$	11.7	21	13	–
Pt$_{62}$Cu$_{38}$/SiO$_2$	5.6	11[7]	17	0.41
Pt$_{35}$Cu$_{65}$/SiO$_2$	4.3	9[3]	18	0.17
Pt$_{16}$Cu$_{84}$/SiO$_2$	3.4	11[2]	23	0.09
Cu/SiO$_2$	–	–	32	–
Cu$_{44}$Pt$_{56}$/SiO$_2$	12.4	21[12]	22	0.55
Pt$_{35}$Cu$_{65}$/SiO$_2$-im	1.1	2	–	–

[a] The dispersion of Pt relative to Pt loadings was calculated by H$_2$ chemisorption data with a stoichiometry of H$_2$/Pt = 2/1. The values in the brackets are the dispersion of Pt relative to the total metal loadings containing both Pt and Cu.

[b] The dispersion of metal particles was estimated according to $D_{metal} = 1/d_{TEM}$.

[c] The percentage of Pt on the surface of bimetallic particles, for example, $[D_{Pt}]/D_{TEM} \times 100 = 50$ indicates that the ratio of surface Pt and Cu equals to 1.

inertness of Cu toward H$_2$ chemisorption. Considering that the H$_2$ chemisorption data were dependent both on the particle size and on the surface compositions, we calculated the dispersion of Pt (D_{Pt}) by normalizing with the amount of Pt or the total amount of Pt and Cu, as seen in column 3 of Table 3. Meanwhile, the dispersion of bimetallic atoms was also estimated from TEM (D_{TEM}), and the result is listed in column 4 of Table 3. By calculating $[D_{Pt}]/D_{TEM}$, one can obtain the percentage of Pt on the surface of bimetallic particles (column 5 of Table 3), with which the enrichment of Pt can be estimated. In other words, the higher the value is, the more enrichment of Pt on the surface. For the series of Pt$_x$Cu$_{100-x}$/SiO$_2$ catalysts, it is clearly seen that with an increase of the Cu content, the particle size decreases and therefore the dispersion of bimetallic atoms (D_{TEM}) increases. On the other hand, although the smaller particle sizes of Pt$_x$Cu$_{100-x}$/SiO$_2$ samples resulted in a higher metal dispersion, the dispersions of Pt relative to the Pt loading in all the bimetallic samples were still lower than that of pure Pt/SiO$_2$ sample due to the inertness of Cu toward H$_2$ chemisorption. Moreover, with an increase of Cu content, the dispersion of Pt relative to the total metals decreases, as a result, the percentage of Pt on the surface ($[D_{Pt}]/D_{TEM}$ values in column 5 of Table 3) decreases following the order of Pt$_{62}$Cu$_{38}$/SiO$_2$ > Pt$_{35}$Cu$_{65}$/SiO$_2$ > Pt$_{16}$Cu$_{84}$/SiO$_2$. Interestingly, the percentages of Pt on the surface were found to be basically the same as those of shell phase compositions obtained by XRD, confirming the Pt-rich core and Cu-rich shell structure derived from our two-step synthesis procedure. Quite different from the series of Pt$_x$Cu$_{100-x}$/SiO$_2$ catalysts, the Cu$_{44}$Pt$_{56}$/SiO$_2$ catalyst exhibited a comparable H$_2$ uptake with that of monometallic Pt/SiO$_2$ catalyst, and the calculated $[D_{Pt}]/D_{TEM}$ was ~55, confirming that the surface of this catalyst is dominated by a Pt^0 rich alloy shell.

IR spectroscopy of CO adsorption is another excellent method to probe the surface species and surface structures of bimetallic catalysts [24]. Fig. 8 shows the DRIFT spectra of CO adsorbed on different samples. On pure Pt/SiO$_2$ sample, a typical linear Pt–CO adsorption vibration frequency is observed at 2084 cm^{-1}, which shifts to 2081 cm^{-1} after purging with He. For Cu-containing samples, it is well known that Cu$^+$ and Cu^0 species have the same vibration frequency of adsorbed CO (at the range of 2100–2200 cm^{-1}) but different strength of adsorption, and CO adsorbed on Cu^0 sites can be easily removed by purging with inert gas like He at room temperature [43,55,56]. Therefore, comparison of spectra of CO adsorption with or without purging with He will help us to identify Cu$^+$ and Cu^0 species in Cu-containing samples. Over pure Cu/SiO$_2$ sample, a predominant ν_{CO} at 2131 cm^{-1} is observed. After purging with He for 20 min, the band intensity decreases greatly with two splitted peaks at 2156 and 2137 cm^{-1} remaining. Thus, a majority of CuO$_x$ should be reduced to Cu^0 with minor Cu$^+$ species residue. For the sample of Pt$_{62}$Cu$_{38}$/SiO$_2$, two

bands at 2084 and 2131 cm^{-1} appear after CO adsorption, however, the purging with He leads to absorption band at 2131 cm^{-1} vanish. It indicates that the surface of Pt$_{62}$Cu$_{38}$/SiO$_2$ contains the main components of Cu^0 and Pt^0. While for Pt$_{35}$Cu$_{65}$/SiO$_2$ and Pt$_{16}$Cu$_{84}$/SiO$_2$ samples, the predominant CO vibration frequency appears at 2131 cm^{-1}, which decreases in strength and splits into two bands at 2156 and 2137 cm^{-1} after purging with He, indicating that both Pt$_{35}$Cu$_{65}$/SiO$_2$ and Pt$_{16}$Cu$_{84}$/SiO$_2$ samples contain a large amount of Cu^0 species on their surface, but still with some Cu$^+$ and Pt^0 species. Over the Cu$_{44}$Pt$_{56}$/SiO$_2$ sample, similar CO vibration bands with those of Pt$_{62}$Cu$_{38}$/SiO$_2$ are observed but with a remarkable red-shift before purging by He, indicating the surface structure of this catalyst is similar to that of Pt$_{62}$Cu$_{38}$/SiO$_2$ but with a higher alloying extent. Our DRIFT spectra results about the surface composition are in good consistence with the H$_2$-chemisorption and TPR results. Besides, in the bimetallic catalysts, a red-shift of linear Pt–CO vibration frequency is observed after He purging, indicative of the electron transfer from Cu to Pt in the alloy shell.

3.4. Hydrodechlorination of 1,2-dichloroethane over different structured catalysts

Hydrodechlorination is an important reaction in environmental catalysis for the conversion of chlorinated hydrocarbon byproducts into industrially important ethylene. Supported Pt–Cu alloy nanocatalysts have been widely investigated for this reaction and Cu-rich alloy has been found to be selective for the formation of ethylene [19,22,24,27,29]. However, little attention has been paid to the effect of bimetallic structures on the catalytic performances. In this work, with the success in the preparation of different structured Pt–Cu bimetallic catalysts, we can investigate the effect of bimetallic Pt–Cu structures on the reactivity in hydrodechlorination reaction. The catalytic performances of different structured catalysts were evaluated with time on stream at two typical temperatures: 275 and 350 °C. As shown in Fig. 9, a relatively stable performance in terms of DCE conversion could be obtained over all the Pt–Cu bimetallic catalysts when the reaction temperature maintained at 275 °C. In contrast, monometallic Pt/SiO$_2$ and Cu/SiO$_2$ had a rapid deactivation. Clearly, alloying Pt with Cu improved the stability of catalysts in hydrodechlorination reaction, in agreement with the results reported previously [24]. The most active catalyst was Cu$_{44}$Pt$_{56}$/SiO$_2$ catalyst, which was followed in an order of Pt$_{62}$Cu$_{38}$/SiO$_2$ > Pt$_{35}$Cu$_{65}$/SiO$_2$ > Pt$_{16}$Cu$_{84}$/SiO$_2$ > Pt$_{35}$Cu$_{65}$/SiO$_2$-im > Pt/SiO$_2$ > Cu/SiO$_2$. This activity order was in good consistence with the surface percentage of Pt in the catalysts (column 5 of Table 3). The more enrichment of Pt is on the surface, the higher activity is for hydrodechlorination. However, pure Pt/SiO$_2$ catalyst exhibited a poor activity, even lower than those of bimetallic catalysts, which is most likely due to the large particle sizes of Pt in this catalyst. Similarly, the low activity of Pt$_{35}$Cu$_{65}$/SiO$_2$-im catalyst can also be ascribed to its large and non-uniform particle sizes.

On the other hand, the different structured catalysts exhibited quite different selectivity to ethylene. Catalysts with a high percentage of Pt on the surface (see column 5 of Table 3), such as Pt$_{62}$Cu$_{38}$/SiO$_2$, Cu$_{44}$Pt$_{56}$/SiO$_2$, and pure Pt/SiO$_2$, gave predominantly ethane, and the ethylene selectivity was almost zero. On the contrary, the pure Cu/SiO$_2$ catalyst gave ethylene selectivity nearly 100%, which is in accordance with the literature [24,25]. For the Pt$_x$Cu$_{100-x}$/SiO$_2$ catalysts, the ethylene selectivity follows the order of Pt$_{16}$Cu$_{84}$/SiO$_2$ > Pt$_{35}$Cu$_{65}$/SiO$_2$ > Pt$_{62}$Cu$_{38}$/SiO$_2$, which is in good agreement with the enrichment of Cu on the surface. That is, the more enriched with Cu of the Pt–Cu alloy shell, the lower capability for H$_2$ chemisorption, and the higher selectivity
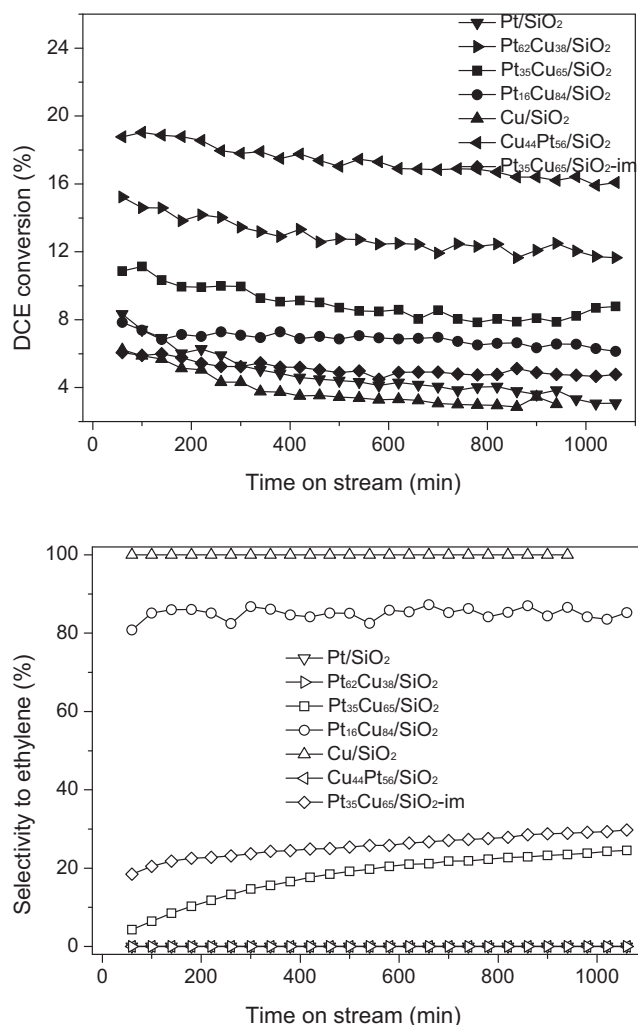
Fig. 9. DCE conversion (solid) and ethylene selectivity (open) with time on stream over different catalysts at 275 °C. Feed composition: 3.3% DCE, 33% H_2, and balance He; flow rate 30 mL/min, space velocity 36,000 $cm^3\,g^{-1}\,h^{-1}$.

Fig. 10. DCE conversion (solid) and ethylene selectivity (open) with time on stream over different catalysts at 350 °C. Feed composition: 3.3% DCE, 33% H_2, and balance He; flow rate 30 mL/min, space velocity 36,000 $cm^3\,g^{-1}\,h^{-1}$.

towards ethylene. In particular, for the $Pt_{16}Cu_{84}/SiO_2$ catalyst, the selectivity to ethylene was nearly 90% and remained stable over 18 h run. This result is significantly better than that reported in literature [24], indicating that the core–shell structure with Cu enriched in the shell is an excellent catalyst in hydrodechlorination reactions.

When the reaction proceeded at a higher reaction temperature, e.g., 350 °C, the stability in terms of DCE conversion and ethylene selectivity changed greatly in comparison with the reaction at 275 °C. As shown in Fig. 10, the pure Cu/SiO_2 catalyst could still achieve an acceptable DCE conversion and a very high selectivity to ethylene at the beginning, however, it deactivated very quickly with the time on stream. The DCE conversion decreased from 39% to 4% while the ethylene selectivity decreased from 94% to 60% after 18 h run. The side product produced on the Cu/SiO_2 catalyst was chloroethylene rather than ethane, indicating incomplete dechlorination. This is in agreement with the literature report that the fast deactivation of Cu catalyst was mainly due to the Cl-poisoning of the Cu sites [15]. While for pure Pt/SiO_2 catalyst, it showed a very high activity at the initial reaction stage, however, its activity declined quickly, with DCE conversion decreasing from 81% to 24% after 2 h reaction. The deactivation of Pt is most likely caused by sintering of particles and coking, as indicated by XRD and TPO characterizations of the used catalyst (Figs. S3 and S4 in supplementary
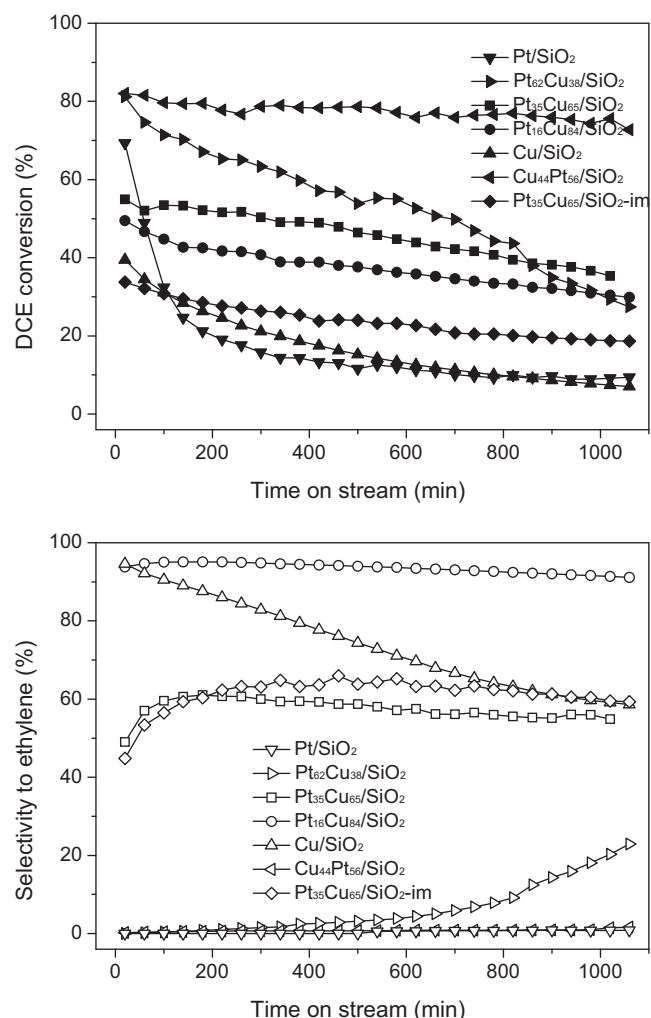
material). For the series of Pt_xCu_{100-x}/SiO_2 catalysts, the enrichment of Cu on the surface resulted in an improved stability in hydrodechlorination reaction. Moreover, the more enrichment of Cu is on the surface, the more stable the catalyst is. For example, the $Pt_{16}Cu_{84}/SiO_2$ catalyst behaved quite stable over 18 h on stream; the selectivity to ethylene decreased only slightly from 95% to 91% while the DCE conversion decreases from 49% to 29%. In contrast, the $Pt_{62}Cu_{38}/SiO_2$ catalyst behaved more like pure Pt/SiO_2; more than half of the DCE conversion was lost during 18 h run. Quite different from $Pt_{62}Cu_{38}/SiO_2$ catalyst, the $Cu_{44}Pt_{56}/SiO_2$ catalyst behaved quite stable even at the reaction temperature of 350 °C due to its outstanding resistance to sintering and coking (see Figs. S3 and S4 in supplementary material). Since the $Cu_{44}Pt_{56}/SiO_2$ catalyst was prepared in a different procedure from the series of Pt_xCu_{100-x} catalysts, Cu and Pt on the surface probably has a higher alloying extent than Pt_xCu_{100-x} catalysts, which can effectively limit the sintering of particles as well as coking on the surface.

4. Conclusion

We successfully synthesized a series of Pt–Cu bimetallic catalysts with different structures and chemical compositions using a two-step method. Compared with co-impregnation method, the two-step method presents a better control in the particle size and structure. For the series of Pt_xCu_{100-x}/SiO_2 catalysts, all the calcined

samples show a core–shell like structure with a Pt core covered or decorated with CuO shell/patches. The CuO shell/patches play an important role in preventing the aggregation of particles during the high-temperature calcination, which results in decreased particle sizes with increasing the Cu content. Upon high temperature reduction, the core–shell like structures remain, but the cores become the Pt-rich alloy phases and the shells become the Cu rich alloys. The formation of the Cu-rich alloys improves the adsorption capabilities of the catalysts compared with pure Cu/SiO_2. In contrast to the series of Pt_xCu_{100-x}/SiO_2 catalysts, the $Cu_{44}Pt_{56}/SiO_2$ catalyst prepared with a reverse deposition sequence presents the core–shell structure with a Cu-rich alloy core and a Pt rich alloy shell. These different structured catalysts exhibit quite different selectivity in the hydrodechlorination of 1,2-dichloroethane. The $Pt_{16}Cu_{84}/SiO_2$ catalyst gave the highest selectivity to ethylene (over 90%) and excellent stability over 18 h run.

Acknowledgement

Appendix A. Supplementary data

Supplementary data associated with this article can be found, in the online version, at http://dx.doi.org/10.1016/j.apcatb.2012.03.020.

References

[1] T.K. Kuhn, K. Hamonts, J.A. Dijk, H. Kalka, W. Stichler, D. Springael, W. Dejonghe, R.U. Meckenstock, Environ. Sci. Technol. 43 (2009) 5263–5269.
[2] I. Ristoiu, K.M. Haydee, T. Ristoiu, J. Environ. Prot. Ecol. 11 (2010) 1229–1238.
[3] M.A. Alvarez-Montero, L.M. Gomez-Sainero, A. Mayoral, I. Diaz, R.T. Baker, J.J. Rodriguez, J. Catal. 279 (2011) 389–396.
[4] S. Ordonez, B.P. Vivas, F.V. Diez, Appl. Catal. B 95 (2010) 288–296.
[5] M.A. Alvarez-Montero, L.M. Gomez-Sainero, M. Martin-Martinez, F. Heras, J.J. Rodriguez, Appl. Catal. B 96 (2010) 148–156.
[6] W. Piechocki, G. Gryglewicz, S. Gryglewicz, J. Hazard. Mater. 163 (2009) 1397–1402.
[7] A. Elola, E. Diaz, S. Ordonez, Environ. Sci. Technol. 43 (2009) 1999–2004.
[8] R.F. Bueres, E. Asedegbega-Nieto, E. Diaz, S. Ordonez, F.V. Diez, Catal. Commun. 9 (2008) 2080–2084.
[9] A. Srebowata, W. Juszczyk, Z. Kaszkur, Z. Karpinski, Catal. Today 124 (2007) 28–35.
[10] M.O. Nutt, J.B. Hughes, M.S. Wong, Environ. Sci. Technol. 39 (2005) 1346–1353.
[11] M. Legawiec-Jarzyna, A. Srebowata, W. Juszczyk, Z. Karpinski, J. Mol. Catal. A 224 (2004) 171–177.
[12] Y.H. Choi, W.Y. Lee, J. Mol. Catal. A 174 (2001) 193–204.
[13] Y.H. Choi, W.Y. Lee, Catal. Lett. 67 (2000) 155–161.
[14] M. Duhamel, E.A. Edwards, Environ. Sci. Technol. 41 (2007) 2303–2310.
[15] N. Barrabes, D. Cornado, K. Foettinger, A. Dafinov, J. Llorca, F. Medina, G. Rupprechter, J. Catal. 263 (2009) 239–246.
[16] W. Juszczyk, J.C. Colmenares, A. Srebowata, Z. Karpinski, Catal. Today 169 (2011) 186–191.
[17] A. Srebowata, M. Sadowska, W. Juszczyk, Z. Kaszkur, Z. Kowalczyk, M. Nowosielska, Z. Karpinski, Catal. Commun. 8 (2007) 11–15.
[18] W.D. Rhodes, J.L. Margitfalvi, I. Borbath, K. Lazar, V.I. Kovalchuk, J.L. d'Itri, J. Catal. 230 (2005) 86–97.
[19] V.Y. Borovkov, D.R. Luebke, V.I. Kovalchuk, J.L. d'Itri, J. Phys. Chem. B 107 (2003) 5568–5574.
[20] W.D. Rhodes, K. Lazar, V.I. Kovalchuk, J.L. d'Itri, J. Catal. 211 (2002) 173–182.
[21] D.R. Luebke, L.S. Vadlamannati, V.I. Kovalchuk, J.L. d'Itri, Appl. Catal. B 35 (2002) 211–217.
[22] L. Vadlamannati, V. Kovalchuk, J. d'Itri, Catal. Lett. 58 (1999) 173–178.
[23] B. Heinrichs, P. Delhez, J.P. Schoebrechts, J.P. Pirard, J. Catal. 172 (1997) 322–335.
[24] H. Xie, J.Y. Howe, V. Schwartz, J.R. Monnier, C.T. Williams, H.J. Ploehn, J. Catal. 259 (2008) 111–122.
[25] L.S. Vadlamannati, D.R. Luebke, V.I. Kovalchuk, J.L. d'Itri, Stud. Surf. Sci. Catal. (2000) 233–238.
[26] N. Job, B. Heinrichs, F. Ferauche, F. Noville, J. Marien, J.P. Pirard, Catal. Today 102 (2005) 234–241.
[27] S. Lambert, F. Ferauche, A. Brasseur, J.P. Pirard, B. Heinrichs, Catal. Today 100 (2005) 283–289.
[28] L. Li, X.D. Wang, A.Q. Wang, J.Y. Shen, T. Zhang, Thermochim. Acta 494 (2009) 99–103.
[29] S. Lambert, B. Heinrichs, A. Brasseur, A. Rulmont, J.P. Pirard, Appl. Catal. A 270 (2004) 201–208.
[30] B. Heinrichs, J.P. Schoebrechts, J.P. Pirard, J. Catal. 200 (2001) 309–320.
[31] J. Kugai, J.T. Miller, N. Guo, C.S. Song, J. Catal. 277 (2011) 46–53.
[32] O.S.G.P. Soares, J.J.M. Órfão, J. Ruiz-Martínez, J. Silvestre-Albero, A. Sepúlveda-Escribano, M.F.R. Pereira, Chem. Eng. J. 165 (2010) 78–88.
[33] O.S.G.P. Soares, J.J.M. Órfão, M.F.R. Pereira, Appl. Catal. B 91 (2009) 441–448.
[34] N.N. Kariuki, X.P. Wang, J.R. Mawdsley, M.S. Ferrandon, S.G. Niyogi, J.T. Vaughey, D.J. Myers, Chem. Mater. 22 (2010) 4144–4152.
[35] H.L. Jiang, Q. Xu, J. Mater. Chem. 21 (2011) 13705–13725.
[36] P. Dash, T. Bond, C. Fowler, W. Hou, N. Coombs, R.W.J. Scott, J. Phys. Chem. C 113 (2009) 12719–12730.
[37] S.H. Zhou, Z. Ma, H.F. Yin, Z.L. Wu, B. Eichhorn, S.H. Overbury, S. Dai, J. Phys. Chem. C 113 (2009) 5758–5765.
[38] S. Marx, A. Baiker, J. Phys. Chem. C 113 (2009) 6191–6201.
[39] D. Wang, A. Villa, F. Porta, L. Prati, D.S. Su, J. Phys. Chem. C 112 (2008) 8617–8622.
[40] S. Zhou, B. Varughese, B. Eichhorn, G. Jackson, K. McIlwrath, Angew. Chem. Int. Ed. 44 (2005) 4539–4543.
[41] X.Y. Liu, A.Q. Wang, X.F. Yang, T. Zhang, C.Y. Mou, D.S. Su, J. Li, Chem. Mater. 21 (2009) 410–418.
[42] X. Liu, A. Wang, X. Wang, C.-Y. Mou, T. Zhang, Chem. Commun. (2008) 3187–3189.
[43] X. Liu, A. Wang, L. Li, T. Zhang, C.-Y. Mou, J.-F. Lee, J. Catal. 278 (2011) 288–296.
[44] X. Liu, A. Wang, T. Zhang, D.-S. Su, C.-Y. Mou, Catal. Today 160 (2011) 103–108.
[45] C.H. Tu, A.Q. Wang, M.Y. Zheng, X.D. Wang, T. Zhang, Appl. Catal. A 297 (2006) 40–47.
[46] C.W. Chiang, A. Wang, B.Z. Wan, C.Y. Mou, J. Phys. Chem. B 109 (2005) 18042–18047.
[47] T. Komatsu, A. Tamura, J. Catal. 258 (2008) 306–314.
[48] H. Tada, A. Takao, T. Akita, K. Tanaka, Chem. Phys. Chem. 7 (2006) 1687–1691.
[49] N. Toshima, Y. Wang, Langmuir 10 (1994) 4574–4580.
[50] A.R. Denton, N.W. Ashcroft, Phys. Rev. A 43 (1991) 3161–3164.
[51] A. Christensen, A.V. Ruban, P. Stoltze, K.W. Jacobsen, H.L. Skriver, J.K. Norskov, F. Besenbacher, Phys. Rev. B 56 (1997) 5822–5834.
[52] A. Sarkar, A. Manthiram, J. Phys. Chem. C 114 (2010) 4725–4732.
[53] H.J. Jang, W.K. Hall, J.L. d'Itri, J. Phys. Chem. 100 (1996) 9416–9420.
[54] D.J. Liu, H.J. Robota, Catal. Lett. 21 (1993) 291–301.
[55] K. Hadjiivanov, T. Tsoncheva, M. Dimitrov, C. Minchev, H. Knozinger, Appl. Catal. A 241 (2003) 331–340.
[56] B. Qiao, A. Wang, J. Lin, L. Li, D. Su, T. Zhang, Appl. Catal. B 105 (2011) 103–110.